

Joint Gaze-Location and Gaze-Object Detection

Danyang Tu, Wei Shen, Wei Sun, Xionghuo Min, Guangtao Zhai

Abstract—This paper proposes an efficient and effective method for joint gaze location detection (GL-D) and gaze object detection (GO-D), *i.e.*, gaze following detection. Current approaches frame GL-D and GO-D as two separate tasks, employing a multi-stage framework where human head crops must first be detected and then be fed into a subsequent GL-D sub-network, which is further followed by an additional object detector for GO-D. In contrast, we reframe the gaze following detection task as detecting human head locations and their gaze followings simultaneously, aiming at jointly detect human gaze location and gaze object in a unified and single-stage pipeline. To this end, we propose GTR, short for Gaze following detection **T**ransformer, streamlining the gaze following detection pipeline by eliminating all additional components, leading to the first unified paradigm that unites GL-D and GO-D in a fully end-to-end manner. GTR enables an iterative interaction between holistic semantics and human head features through a hierarchical structure, inferring the relations of salient objects and human gaze from the global image context and resulting in an impressive accuracy. Concretely, GTR achieves a 12.1 mAP gain (25.1%) on GazeFollowing and a 18.2 mAP gain (43.3%) on VideoAttentionTarget for GL-D, as well as a 19 mAP improvement (45.2%) on GOO-Real for GO-D. Meanwhile, unlike existing systems detecting gaze following sequentially due to the need for a human head as input, GTR has the flexibility to comprehend any number of people’s gaze followings simultaneously, resulting in high efficiency. Specifically, GTR introduces over a $\times 9$ improvement in FPS and the relative gap becomes more pronounced as the human number grows.

I. INTRODUCTION

GAZE following is one of the extraordinary human abilities to precisely track others’ gaze directions and identify their gaze targets. In real-world scenarios, the human visual system operates with speed and precision, allowing us to perform complex vision tasks with little conscious thoughts, such as effortlessly understanding the behavioural intentions of others. Similarly, fast and accurate gaze following detection algorithms will enable machines to better interpret human behaviors, thereby presenting a significantly potential in various human-centric vision tasks, such as saliency prediction [24], human action detection [33], and human-object interaction detection [45], among others [47].

Existing detection systems frame gaze following detection as two separate tasks, *i.e.*, detecting *where* each human is looking at (gaze location detection, GL-D) [6, 11, 38] and detecting *what* each human is looking at (gaze object detection, GO-D) [37, 44]. Specifically, the former aims to predict the gaze location of each human (*i.e.*, a heatmap, the magnitude of different locations indicates the possibility that the location is the gaze point), while the latter further identify the category of the object being looked at (*i.e.*, a bounding box with object label).

Despite varying in targets, current gaze following detection systems invariably share a similar multi-stage framework. As

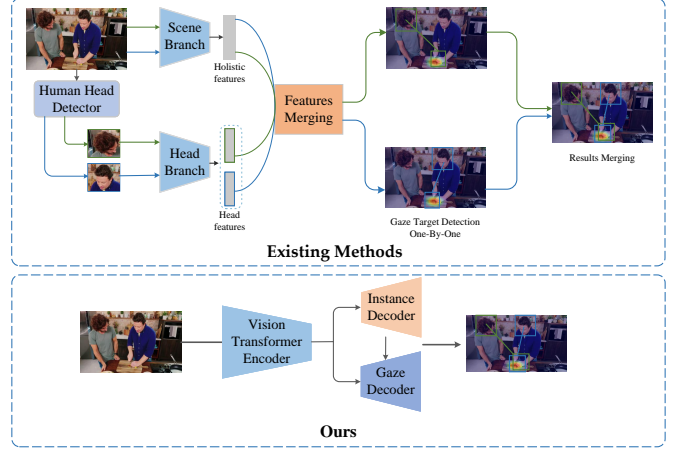


Fig. 1: **Existing methods vs. our model.** Existing methods conventionally execute a multi-stage framework, yielding less competitive performance in model efficiency and limiting model precision due to error accumulation. In comparison, our method dispenses with any additional modules, leading to the first unified and single-stage pipeline for gaze-following detection.

shown in Fig. 1, taking both a scene image and a given human head crop as inputs, recent GL-D approaches conventionally adopt a scene branch to extract holistic cues and another parallel head branch to capture head pose features. These holistic and head features are subsequently agglomerated to predict the gaze location of the given human, which is followed by a post-processing module to merge all humans’ gazes in an identical scene onto one canvas. On this basis, GO-D methods further leverage an additional off-the-shelf object detector to recognize the instances being staring at. These methods are highly instructive since they demonstrate the ability of machines to estimate human gaze targets directly from images or videos, without the necessity of any specialized sensors, such as monitor-based or wearable eye trackers.

Nevertheless, these complex pipelines work slowly and show inferior precision due to several major limitations: (I) Current methods invariably take as inputs a human head crop and a scene image, where the former is manually labeled by humans. Therefore, in real-world applications, an additional human head detector is essential to detect human head crops firstly, which enforces a two-stage framework that struggles with head crops extraction, yielding less competitive performance in model efficiency. Moreover, such a two-stage and cascaded pipeline potentially amplifies the impact of false detection by human head detector, *i.e.*, a minor head detection error can fail the subsequent gaze following reasoning (Sec. IV-D). (II) Taking a given head crop as input, existing methods are restricted to detect gaze following sequentially, *i.e.*, only one person’s gaze target can be predicted at a

time. Such limitation further degrades model efficiency when handling with multiple humans in an identical scene, as the detection process is forced to be repeatedly performed even if the holistic scene features remain unchanged (Sec. IV-D). (III) Existing methods extract holistic scene contexts and head pose features separately, lacking contextual relational reasoning for interactions between them (Sec. IV-E). (IV) There is no an unified paradigm that enables to detect gaze locations and gaze objects simultaneously in an end-to-end manner, *i.e.*, without using any additional components, including but not limited to the additional object detectors.

To alleviate the above limitations, we reframe gaze following detection as a set-based prediction problem, straight from image pixels to gaze point coordinates and gaze objects, leading to a fast and accurate detection system. Therefore, we propose **GTR**, a novel **G**aze following detection **TR**ansformer that unites human gaze location detection and gaze object detection in an fully end-to-end framework for the first time. The superiority of our method is listed as follows:

First, GTR is extremely fast with two novel designs: 1) We abandon the practice of using human head crops as inputs and instead leverage them as the prediction targets of the GTR. Not only does it eliminate the utilization of an extra head detector, but it also allows GTR to flexibly predict the gaze followings of humans with an arbitrary number at once. Concretely, GTR’s outputs can be formulated as N human-gaze-following (HGF) triplets in the format of `< head location, gaze location, gaze object >`, where N counts the number of humans in a given image. 2) GTR dispenses with all offline components, such as post-processing module and the additional object detector, and is designed as a visual encoder followed by a two-branch decoder, which is organized as a single-stage pipeline and can be trained in a completely end-to-end manner. Hence, taking as input an image containing 6 people, our GTR is more than nine times faster than prior methods, and the relative FPS gap is more evident as the number of humans in an image grows.

Second, GTR shows significant precision, especially in practical scenarios with various distortions. With Transformer as key component, GTR outperforms previous methods with an excellent capability to capture long-range gaze behaviours by enhancing the contextual relational reasoning. Specifically, GTR starts with performing a visual encoder to extract global memory features, followed by a two-branch decoder (*i.e.*, human decoder and gaze following decoder), where the former recognizes all humans in an image and the latter infers their gaze locations and objects. Meanwhile, a guided mechanism is developed to differentiate different human-gaze-object pairs by dynamically agglomerating the human query and the global scene context, which enables an iterative and hierarchical interaction between human decoder and gaze following decoder. Finally, the HGF triplets are predicted using several multi-layer perceptrons in parallel. Besides, we devise a new objective function, which unites the GL-D and GO-D in an unified framework and allows the model to be trained in an end-to-end manner. Extensive experimental results show that GTR outperforms existing methods by significant margins. Specifically, GTR realizes a **12.1** mAP gain (**25.1%**)

on GazeFollowing [31] and a **18.2** mAP gain (**43.3%**) on VideoAttentionTarget [6] for GL-D, as well as a **19.0** mAP improvement (**45.2%**) on GOO-Real [37] for GO-D.

The remainder of this paper is organized as follows. Section II reviews the prior works related to ours. Section III explores the solution of uniting GL-D and GO-D in a single-stage pipeline. Section IV studies the efficiency and effectiveness of our proposed method. Section V discusses the failed cases of our method and the potential solutions. Section VI gives the concluding remarks.

II. RELATED WORK

Eye tracking was widely explored in psychological research [7, 17, 22, 48, 52, 54] and saliency prediction tasks [9, 12, 18, 20, 24, 30, 46], which aims to predict the eye fixations of an observer looking at a given picture, with the observer outside the picture. Specifically, eye tracking systems were typically built on sophisticated monitor-based or wearable eye tracking devices. As these devices require delicate pre-commissioning, the observer is expected to maintain in a stationary position with a well-calibrated posture during experiments. In contrast, the goal of gaze following detection is to estimate what is being looked at by a person inside a picture or video [31], *i.e.*, detecting human attentions in an unconstrained manner. Therefore, observers are allowed to act freely in an arbitrary scenario in gaze following detection systems and we observe them in a third-person perspective. With this, gaze following detection is a more practical vision task that can be use in many daily scenarios, such as understanding human-human interactions and human-object interactions.

Gaze following detection was first proposed in [31], which built GazeFollowing, a large-scale dataset annotated with the location of where people in images are looking. On this basis, Chong *et al.* [5] further solved the problem of out-of-frame gaze targets prediction (*i.e.*, the gaze location of someone is not in the given image) by predicting saliency map and learning gaze angle simultaneously. Meanwhile, the precision of image-based gaze target prediction was continually improved by leveraging other different auxiliary information, such as body pose [13], sight lines [25, 49], depth [11] and etc. In addition to detecting gaze following in image, Chong *et al.* [6] proposed a new framework to understanding human gaze following from videos, which models the dynamic interaction between the scene and head features using attention mechanism and infers time-varying attention targets. They also built a new annotated dataset named VideoAttentionTarget, which contains complex and dynamic patterns of real-world gaze behavior. There are also other related works, including but not limited to [4, 19, 20, 22, 24, 54].

More recently, [37] presented a new task, gaze object detection, where one must infer the bounding box of the object gazed at by the target person. It also propose a new Gaze On Objects (GOO) dataset that is composed of a large set of synthetic images (GOO-Synth) supplemented by a smaller subset of real images (GOO-Real) of people looking at objects in a retail environment. On this basis, Wang *et al.* [44] propose a new method GaTector for gaze object detection,

which leveraged an additional object detector (YOLOV4 [1]) to recognize target objects.

Despite being ingenious, these methods invariably took manually annotated human heads as inputs, which enforces a multi-stage pipeline that inevitably compromises their efficiency. Besides, a unified framework to jointly detect human gaze location and human gaze object in an end-to-end manner awaits further exploration.

Transformer was originated from the domain of natural language processing [42], which has recently started to revolutionize the computer vision community. In ViT [8], the first vision Transformer, an image is first divided into 16×16 local patches. Along with an additional class token, these local patches are fed into a Transformer encoder, which is organized as several identical self-attention layers, allowing the class token to capture long-range contextual information. Finally, taking the class token as input, a MLP is employed to predict the possible category. Besides, Transformer has also shown great potential in many other vision tasks, including but not limited to [3, 34, 38–41, 50, 53]. These methods share a similar DETR [2]-like framework. Specifically, in a DETR-like framework, a ResNet [14] backbone is first used to capture high-level visual features. Then, along with additional position embeddings, these visual features are fed into a Transformer-encoder to capture global memory features. After that, a set of learnable positional embeddings, named object queries, is responsible for interacting with the global memory features and aggregating information through several interleaved cross-attention and self-attention modules. Eventually, these object queries, decoded by a feed-forward Network (FFN), directly correspond to the final predictions. However, although Transformer has demonstrated great capability in many vision tasks, there is no Transformer-based method for gaze following detection. To the best of our knowledge, we are the first to introduce the Transformer into the domain of gaze following detection.

III. METHODS

A. Problem Reformulation

Given an image $\mathbf{x} \in \mathbb{R}^{3 \times H \times W}$ that contains one or more humans as the input, we redefine gaze following detection as a problem of locating of all humans at one time, as well as predicting of their gaze locations and objects. For convenience, the location of i -th human \mathbf{I}_h^i is denoted as his/her head location since it is available in existing datasets. Concretely, we represent a human's head location as a rectangular bounding box $([x_{tl}, y_{tl}], [x_{br}, y_{br}])$, where the subscripts tl and br indicate top-left and bottom-right, respectively. In addition, the gaze location \mathbf{g}_l^i of the i -th human is represented as a Gaussian heatmap, of which the gaze point is located in the center. Meanwhile, we denote the gaze object of the i -th human as \mathbf{g}_o^i , which consists of a bounding box and an object label. In this way, our new problem can be formulated as maximizing a joint *posteriori* of the output triplets $\langle \mathbf{I}_h, \mathbf{g}_l, \mathbf{g}_o \rangle$ on the given image \mathbf{x} :

$$\mathcal{T}^* \doteq \max_{\mathcal{T}} \prod_{i=1}^N p(\langle \mathbf{I}_h^i, \mathbf{g}_l^i, \mathbf{g}_o^i \rangle | \mathbf{x}), \quad (1)$$

where N can be an arbitrary constant that counts the number of the humans in \mathbf{x} and \mathcal{T}^* refers to the optimal model.

It is worth to emphasize that our new formulation is quite different from the traditional gaze following detection problem [4–6, 11, 19, 20, 22, 24, 31, 54], which demands both scene image \mathbf{x} and a given human head crop \mathbf{x}_h^i as inputs. As aforementioned, it can only predict one individual's gaze location or object $\mathbf{I}_g^i / \mathbf{o}_g^i$ at a time, which is formulated as:

$$\mathcal{T}_{cls}^* \doteq \max_{\mathcal{T}_{cls}} p(\mathbf{I}_g^i / \mathbf{o}_g^i | \mathbf{x}, \mathbf{x}_h^i), \quad (2)$$

where i ranges from 1 to N . Built on this formulation, current methods handle a same image as N different cases if there are N different humans in the image. In comparison, our new formulation introduces a more ambitious problem, but it renders the task of gaze following detection more pertinent to practical demands, enhancing its applicability in real-world scenarios.

B. Network Architecture

In this subsection, we aim to provide the first paradigm that enables gaze location and gaze object to be detected in a unified and end-to-end manner, *i.e.*, our novel GTR.

As illustrated in Fig. 2, GTR is organized as a visual encoder followed by two-branch decoders architecture. In visual encoder, we first adopt a CNN-based backbone to extract higher-level visual features \mathbf{V}_b , which are subsequently enhanced by a Transformer encoder to capture sequenced global memory features \mathbf{V}_e . Then, we perform two-branch decoders, *i.e.*, human decoder and gaze-following decoder, to detect HGF triplets. Taking \mathbf{V}_e as inputs, the human decoder detects all humans through the human query set \mathbf{Q}_h . Meanwhile, we design a weight Guided Embedding (w-GE) \mathbf{P}_w to model the relations of all human queries with different regions in the scene. In the gaze-following decoder, we first generate gaze-following queries $\{\mathbf{Q}_g^l\}_{l=1}^L$ for each gaze-following decoder layer by dynamically agglomerating human queries with global context based on the w-GE $\{\mathbf{P}_w^l\}_{l=1}^L$ from the corresponding human decoder layer, where L denotes the number of layers. Namely, the gaze-following decoder interacts with human decoder iteratively and hierarchically, which enables a hierarchical and dynamical information propagation from human decoder to gaze following decoder, allowing the latter to comprehend HGF triplets under the guidance of human features and holistic context. Finally, the HGF prediction results are generated by several multi-layer preceptions.

Visual encoder. We follow the standard query-based Transformer detector [2] to adopt a CNN equipped with a vision Transformer encoder [8] architecture as the visual encoder. Concretely, given an input image $\mathbf{x} \in \mathbb{R}^{3 \times H \times W}$ containing an arbitrary number of humans, we first perform a ResNet [15] as backbone to extract a downsampled feature map $\mathbf{V}_{\text{CNN}} \in \mathbb{R}^{2048 \times \frac{H}{32} \times \frac{W}{32}}$, which is subsequently fed into a projection convolution layer with a kernel size of 1×1 to reduce the dimension from 2048 to 256, leading to a new feature map $\mathbf{V}'_{\text{CNN}} \in \mathbb{R}^{256 \times \frac{H}{32} \times \frac{W}{32}}$. Following that, a flatten operator is used to collapse the spatial dimension into one, leading

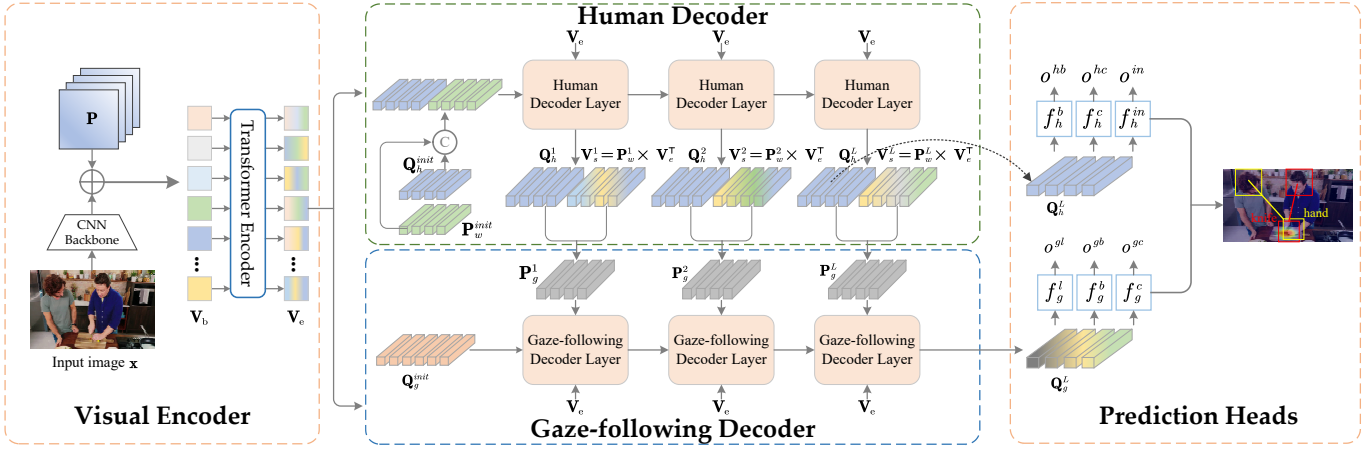


Fig. 2: **Pipeline of our GTR.** The GTR is organized as a visual encoder equipped with two-branch decoders architecture. Given an image, the visual encoder is first applied to extract the global visual features. Then, these global visual features are fed into the subsequent two branches, *i.e.*, human decoder and gaze following decoder, to localize human heads and reason their gaze followings through learnable queries, respectively. Meanwhile, we diversify a weight Guided Embedding (w-GE) to enable an iterative and hierarchical connection between these two decoders, leading to a dynamical interaction between human head features and holistic scene context. Finally, the human head crops and gaze following instances are predicted using several prediction heads in parallel.

to sequenced features $\mathbf{V}_b \in \mathbb{R}^{256 \times \frac{HW}{32 \cdot 32}}$. Finally, a Transformer encoder containing six identical layers is employed to enhance the \mathbf{V}_b with richer contextual information, where each layer is built upon a multi-head self-attention (MSA) module and a feed-forward network (FFN). Meanwhile, a cosine positional encoding $\mathbf{P} \in \mathbb{R}^{256 \times \frac{HW}{32 \cdot 32}}$ is additionally fed into the encoder to supplement the positional information as the Transformer architecture is permutation invariant. After the CNN-Transformer combined visual encoder, we eventually extract sequenced and global visual features $\mathbf{V}_e \in \mathbb{R}^{256 \times \frac{HW}{32 \cdot 32}}$ from the input image \mathbf{x} for the following tasks.

Human decoder. Our human decoder transforms N_h^q human queries by stacking L_h decoder layers consisting of self-attention and cross-attention mechanisms. Simultaneously, it is also expected to learn a set of weight Guided Embeddings (w-GE) for the subsequent holistic context agglomeration. As Fig 2 shown, the l -th human decoder layer takes three parameters as inputs: 1) Global visual features \mathbf{V}_e from the visual encoder, which aims at providing holistic context. 2) Human queries $\mathbf{Q}_h^l \in \mathbb{R}^{N_h^q \times C_q}$, a set of learnable parameters applied to highlight different human instances by iterative learning. Besides, to make these human queries distinct, we additionally add a set of learnable embedding $\mathbf{P}_h^l \in \mathbb{R}^{N_h^q \times C_q}$ to them, serving for extracting the interrelations between all humans instances. 3) Weight Guided Embedding (w-GE) $\mathbf{P}_w^l \in \mathbb{R}^{N_h^q \times C_q}$. After CNN backbone, an image is downsampled by 32×32 , leading to total $\frac{HW}{32 \cdot 32}$ image patches with resolution of 32×32 (each pixel of the feature map from the last layer of ResNet has a receptive field of 32×32). Therefore, the n -th vector $\mathbf{p}_w^{(l,n)} \in \mathbb{R}^{1 \times C_q}$ in \mathbf{P}_w^l aims to learn the relations between the n -th human instance with each patch, *i.e.*, a local region, in the global scene. Here, $C_q = \frac{HW}{32 \cdot 32}$, *i.e.*, the number of image patches. Formally, the human decoder is

organized as:

$$[\hat{\mathbf{Q}}_h^l; \hat{\mathbf{P}}_w^l] = \text{MSA}([\tilde{\mathbf{Q}}_h^l; \mathbf{P}_w^l]), \quad (3)$$

$$[\hat{\mathbf{Q}}_h^l; \hat{\mathbf{P}}_w^l] = \text{MCA}([\hat{\mathbf{Q}}_h^l; \hat{\mathbf{P}}_w^l], \mathbf{V}_e), \quad (4)$$

$$[\hat{\mathbf{Q}}_h^l; \hat{\mathbf{P}}_w^l] = \text{FFN}([\hat{\mathbf{Q}}_h^l; \hat{\mathbf{P}}_w^l]), \quad (5)$$

where $\text{MSA}(\cdot)$ and $\text{MCA}(\cdot, \cdot)$ refer to multi-head self-attention and multi-head cross-attention respectively. $[\cdot]$ denotes concatenation operator. $\tilde{\mathbf{Q}}_h^{init}$ is initialized as the sum of \mathbf{Q}_h^l and \mathbf{P}_h^l . Concretely, we initialize \mathbf{Q}_h^{init} as zeros and \mathbf{P}_h^{init} , \mathbf{P}_w^{init} as normal gaussian embeddings for the first layer, while the other layers take the outputs of previous layer as inputs:

$$\tilde{\mathbf{Q}}_h^1 = \tilde{\mathbf{Q}}_h^{init} = \underbrace{\text{Zeros}(N_h^q, C_q)}_{\mathbf{Q}_h^{init}} + \underbrace{\text{Embedding}(N_h^q, C_q)}_{\mathbf{P}_h^{init}}, \quad (6)$$

$$\mathbf{P}_w^1 = \mathbf{P}_w^{init} = \text{Embedding}(N_h^q, C_q), \quad (7)$$

$$[\tilde{\mathbf{Q}}_h^l; \mathbf{P}_w^l] = [\hat{\mathbf{Q}}_h^{l-1}; \hat{\mathbf{P}}_w^{l-1}] \quad \text{if } l > 1. \quad (8)$$

Note that we omit the modules of residual connection and normlization in the above equations for convenience. Besides, in Fig 2, we omit the \mathbf{P}_h^{init} for conciseness.

Gaze-following decoder. The goal of the gaze-following decoder is to predict where and what of each human is looking at, which demands of sufficient interaction between human features and global scene contexts. Specifically, the gaze-following decoder shares a similar architecture with human decoder, which is organized as a hierarchy of L_g Transformer decoder layers. By design, $L_g = L_h = L$, so we still use l to indicate the index of different layers. Then, for the l -th gaze following decoder layer, it also takes three elements as inputs: 1) The global visual features \mathbf{V}_e . 2) Gaze following queries \mathbf{Q}_g^l , which are also learnable parameters that initialized as zeros. 3) Guided agglomeration \mathbf{P}_g^l of human features and scene contexts. Concretely, we first agglomerate holistic fea-

tures dynamically based on the learned inner-relations between different human instances and the whole scene via

$$\mathbf{V}_s^l = \mathbf{P}_w^l \times \mathbf{V}_e^\top, \quad (9)$$

where \mathbf{P}_w^l is the updated w-GE in the l -th human decoder layer, which attends to the potential salient regions. Namely, \mathbf{V}_s^l is a selective agglomeration of global context that highlighted by human decoder. Subsequently, the \mathbf{P}_g^l can be obtained as:

$$\mathbf{P}_g^l = W_g[\hat{\mathbf{Q}}_h^l; \mathbf{V}_s^l]. \quad (10)$$

Specifically, $\hat{\mathbf{Q}}_h^l$ are the intermediate human features extracted by the l -th human decoder layer (Equation (5)) and W_g are learnable weights of a linear layer. $\{\mathbf{P}_g^l\}_{l=1}^L$ for different gaze following decoder layers contain different levels of human features and different levels of holistic features, enabling a hierarchical and dynamical interaction of human features and scene contexts for the gaze following decoder. Finally, the gaze following decoder can be calculated as:

$$\hat{\mathbf{Q}}_g^l = \text{FFN}(\text{MCA}(\text{MSA}(\mathbf{Q}_g^l + \mathbf{P}_g^l), \mathbf{V}_e)), \quad (11)$$

$$\mathbf{Q}_g^1 = \mathbf{Q}_g^{\text{init}} = \text{Zeros}(N_g^q, C_q), \quad (12)$$

$$\mathbf{Q}_g^l = \hat{\mathbf{Q}}_g^{l-1} \quad \text{if } l > 1. \quad (13)$$

Intuitively, \mathbf{P}_g^l are explicit position encodings, which contain the features of different humans and the relevant scene contexts, guiding the gaze following queries \mathbf{Q}_g^l to attend to different locations and objects for different humans.

Prediction heads. We define each ground-truth HGF instance by the following five vectors: a human-head-bounding-box vector normalized by the corresponding image size $\mathbf{t}^{hb} \in [0, 1]^4$; a watch-in-out (whether the gaze target is located inside the scene image or not) binary one-hot vector $\mathbf{t}^{io} \in \{0, 1\}^2$; a normalized gaze-object-bounding-box vector $\mathbf{t}^{gb} \in [0, 1]^4$; a gaze-object-category one-hot vector $\mathbf{t}^{gc} \in \{0, 1\}^{N_o+1}$; and a gaze location heatmap vector $\mathbf{t}^{gl} \in [0, 1]^{H_o \times W_o}$, where $H_o \times W_o$ denotes the spatial resolution of the output gaze heatmap. N_o is the number of object categories and the last element (the $(N_o + 1)$ -th element) in \mathbf{t}^{gc} indicates *no-object*, *i.e.*, someone is looking at background.

On this basis, we perform several multi-layer perception (MLP) on each human query and gaze-following query to decode the final HGF instance. Concretely, taking as inputs the human queries extracted by the last human decoder layer \mathbf{Q}_h^L , we perform an one-layer MLP branch f_{io} and a three-layer MLP branch f_h^b to predict the watch-in-out confidence \mathbf{o}^{io} and human head bounding box \mathbf{o}^{hb} , respectively. Note that we additionally adopt an one-layer MLP branch f_h^c to estimate the human confidence \mathbf{o}^{hc} , *i.e.*, whether the predicted human-head-bounding-box is a true human head or not. Synchronously, we feed the gaze following queries captured by the last gaze following decoder layer \mathbf{Q}_g^L to a five-layer MLP branch f_g^l , a one-layer MLP branch f_g^c and a three-layer MLP f_g^b to predict human gaze location \mathbf{o}^{gl} , human gaze-object probability \mathbf{o}^{gc} and human-gaze-object bounding box \mathbf{o}^{gb} , respectively. We use a softmax function for both

f_h^c , f_{io} , f_g^c and a sigmoid function for f_h^b , f_g^b , f_g^l .

C. Loss Calculation

The loss calculation is composed of two stages: the bipartite matching between ground-truths and model predictions, which is followed by the loss computation for the matched pairs.

Bipartite matching. We following the training procedure of DETR [2] to use the Hungarian algorithm [23] for the bipartite matching, which is designed to obviate the process of suppressing over-detection. First, we pad the ground-truth of HGF instances with ϕ (no instance) to make the size of ground-truths set becomes N_q .

As illustrated in Fig 2, our GTR outputs a fixed-size set of N_q HGF instance predictions, and we denote them as $\mathbf{O} = \{\mathbf{o}_j\}_{j=1}^{N_q}$, in which the j -th prediction $\mathbf{o}_j = \{\mathbf{o}_j^{hb}, \mathbf{o}_j^{hc}, \mathbf{o}_j^{io}, \mathbf{o}_j^{gl}, \mathbf{o}_j^{gb}, \mathbf{o}_j^{gc}\}$. Meanwhile, we use $\mathbf{T} = \{\mathbf{t}_k\}_{k=1}^{N_{gt}} \cup \{\mathbf{t}_n = \phi\}_{n=N_{gt}+1}^{N_q}$ to represent the padded ground-truths and $\mathbf{t}_k = \{\mathbf{t}_k^{hb}, \mathbf{t}_k^{io}, \mathbf{t}_k^{gl}, \mathbf{t}_k^{gb}, \mathbf{t}_k^{gc}\}$ (human confidence has no ground-truth). N_{gt} is the real number of HGF instances in a given image. By design, N_q is always larger than N_{gt} . On this basis, the matching process can be denoted as an injective function: $\omega_{\mathbf{T} \rightarrow \mathbf{O}}$, where $\omega(i)$ is the index of predicted HGF instance assigned to the i -th ground-truth. We define the matching cost as:

$$\mathcal{L}_{\text{cost}} = \sum_i^{N_q} \mathcal{L}_{\text{match}}(\mathbf{t}_i, \mathbf{o}_{\omega(i)}), \quad (14)$$

where $\mathcal{L}_{\text{match}}(\mathbf{t}_i, \mathbf{o}_{\omega(i)})$ is a matching cost between the i -th ground-truth and the $\omega(i)$ -th prediction. Formally, $\mathcal{L}_{\text{match}}(\mathbf{t}_i, \mathbf{o}_{\omega(i)})$ consists of three types of cost, including cost for human head prediction \mathcal{L}_h , cost for gaze-location prediction \mathcal{L}_{gl} , and cost for gaze-object prediction \mathcal{L}_{go} , *i.e.*,

$$\mathcal{L}_{\text{match}}(\mathbf{t}_i, \mathbf{o}_{\omega(i)}) = \sigma_1 \mathcal{L}_h + \sigma_2 \mathcal{L}_{gl} + \sigma_3 \mathcal{L}_{go}. \quad (15)$$

Firstly,

$$\mathcal{L}_h = \alpha_h^1 \mathcal{L}_h^b + \alpha_h^2 \mathcal{L}_h^c, \quad (16)$$

where \mathcal{L}_h^b is human-head-bounding-box regression loss, which is a weighted sum of GIoU [32] loss and L_1 loss:

$$\mathcal{L}_h^b = \beta_{hb}^1 \left\| \mathbf{t}_i^{hb} - \mathbf{o}_{\omega(i)}^{hb} \right\| - \beta_{hb}^2 \text{GIoU}(\mathbf{t}_i^{hb}, \mathbf{o}_{\omega(i)}^{hb}). \quad (17)$$

\mathcal{L}_h^c indicates is-head loss, which is defined as:

$$\mathcal{L}_h^c = -\mathbf{o}_{\omega(i)}^{hc}(0), \quad (18)$$

where the first element $\mathbf{o}^{hc}(0)$ of \mathbf{o}^{hc} indicates the model confidence about the detected human instance is positive.

Secondly,

$$\mathcal{L}_{gl} = \alpha_{gl}^1 \mathcal{L}_g^l + \alpha_{gl}^2 \mathcal{L}^{io}, \quad (19)$$

where \mathcal{L}_g^l is a L_2 distance between predicted human gaze location and the ground-truth one:

$$\mathcal{L}_g^l = \left\| \mathbf{t}_i^{gl} - \mathbf{o}_{\omega(i)}^{gl} \right\|_2. \quad (20)$$

\mathcal{L}^{io} stands for watch-in-out loss, which is calculated as:

$$\mathcal{L}^{io} = -\mathbf{o}_{\omega(i)}^{io}(0), \quad (21)$$

where the first element $\mathbf{o}_{\omega(i)}^{io}(0)$ of $\mathbf{o}_{\omega(i)}^{io}$ similarly refers to the model confidence about the detected human gaze point is located inside the image.

Finally,

$$\mathcal{L}_{go} = \alpha_{go}^1 \mathcal{L}_g^b + \alpha_{go}^2 \mathcal{L}_g^c, \quad (22)$$

where \mathcal{L}_g^b is gaze-object bounding box regression loss, which is also a weighted sum of GIoU loss and L_1 loss:

$$\mathcal{L}_g^b = \beta_{gb}^1 \left\| \mathbf{t}_i^{gb} - \mathbf{o}_{\omega(i)}^{gb} \right\| - \beta_{hb}^2 \text{GIoU}(\mathbf{t}_i^{gb}, \mathbf{o}_{\omega(i)}^{gb}). \quad (23)$$

\mathcal{L}_g^c represents object recognition cost, which is defined as:

$$\mathcal{L}_g^c = -\mathbf{o}_{\omega(i)}^{gc}(k) \quad s.t. \quad \mathbf{t}_i^{gc}(k) = 1, \quad (24)$$

where the k -th element of $\mathbf{o}_{\omega(i)}^{gc}$ is the probability that the model predicts the gaze object as the ground-truth category.

We then leverage the Hungarian algorithm to determine the optimal assignment $\hat{\omega}$ among the set of all possible permutations of N_q elements Ω_{N_q} . It can be formulated as:

$$\hat{\omega} = \arg \min_{\omega \in \Omega_{N_q}} \mathcal{L}_{cost}. \quad (25)$$

Object function. After the optimal one-to-one matching between the ground-truths and the predictions is found, the loss to be minimized in the training phase is calculated as:

$$\mathcal{L} = \eta_1 \mathcal{L}_1 + \eta_2 \mathcal{L}_2 + \eta_3 \mathcal{L}_u + \eta_4 \mathcal{L}_c, \quad (26)$$

$$\mathcal{L}_1 = \frac{1}{|\bar{\Phi}|} \sum_{i=1}^{N_q} \mathbb{1}_{\{i \notin \Phi\}} \left[\left\| \mathbf{t}_i^{hb} - \mathbf{o}_{\hat{\omega}(i)}^{hb} \right\| + \left\| \mathbf{t}_i^{gb} - \mathbf{o}_{\hat{\omega}(i)}^{gb} \right\| \right], \quad (27)$$

$$\mathcal{L}_2 = \frac{1}{|\bar{\Phi}|} \sum_{i=1}^{N_q} \mathbb{1}_{\{i \notin \Phi\}} \left[\left\| \mathbf{t}_i^{gl} - \mathbf{o}_{\hat{\omega}(i)}^{gl} \right\|_2 \right], \quad (28)$$

$$\mathcal{L}_u = \frac{1}{|\bar{\Phi}|} \sum_{i=1}^{N_q} \mathbb{1}_{\{i \notin \Phi\}} \left[2 - \text{GIoU}(\mathbf{t}_i^{hb}, \mathbf{t}_{\hat{\omega}(i)}^{hb}) - \text{GIoU}(\mathbf{t}_i^{gb}, \mathbf{o}_{\hat{\omega}(i)}^{gb}) \right], \quad (29)$$

$$\mathcal{L}_c = \frac{1}{N_q} \sum_{i=1}^{N_q} \left\{ \mathbb{1}_{\{i \notin \Phi\}} \left[-\log \mathbf{o}_{\hat{\omega}(i)}^{gc}(k) \right] + \mathbb{1}_{\{i \in \Phi\}} \left[-\log \mathbf{o}_{\hat{\omega}(i)}^{gc}(N_o + 1) \right] \right\} \quad s.t. \quad \mathbf{t}_i^{gc}(k) = 1, \quad (30)$$

where Φ is a set of ground-truth indices that correspond to ϕ and $\bar{\Phi}$ is its complementary set. Note that our new loss is quite different from the prior one (typically a simple L_2 loss), which demonstrates a desirable effectiveness (Sec. IV).

IV. EXPERIMENTS

A. Datasets & Evaluation Metrics

Datasets. We train and test our model for GL-D on both Gaze-Following [31] dataset and VideoAttentionTarget [6] dataset.

Specifically, we use every single frame in VideoAttentionTarget as input during the training process, without considering the temporal information. Therefore, to avoid overfitting, for every five continuous frames from the training set of VideoAttentionTarget which have no obvious appearance differences, we randomly select one for training since they have almost the same gaze target. For testing, we still use all images in the testing set.

Meanwhile, we use GOO [37] dataset to evaluate the performance of our model for GO-D. Concretely, GOO contains annotations of bounding boxes for all gaze objects, which are labeled with 24 different categories. Additionally, GOO consists of two different subsets, *i.e.*, GOO-Synth that contains 192,000 synthetic images and GOO-Real that contains 9,552 real images.

Moreover, one of objectives of our proposed model is to predict the locations of different individuals. Therefore, the head locations in existing dataset annotations are no longer used as inputs but as ground-truths. Besides, previous works predict the gaze target for different subjects in an identical scene on a case-by-case basis, which results in each image being assigned with M annotations, and M is the number of people in an image. Unlike that, we merge the annotations of the same image into the same format as COCO [26] object detection since we aim to predict them all at one time.

Evaluation metric. In this work, we have to evaluate the performance of proposed model in terms of both gaze following detection (GL-D and GO-D) and human position detection.

First, we follow the standard evaluation protocols, as in [6, 31, 37], to report the results of GL-D in terms of AUC and L_2 distance. For AUC: the final heatmap provides the prediction confidence score which is evaluated at different thresholds in the ROC curve. The area under curve (AUC) of the ROC is reported [6]. In terms of distance: L_2 distance between the annotated target location and the prediction given by the pixel having the maximum value in the heatmap, with image width and height normalized to 1, is reported. Specifically, since the ground truth for GazeFollowing may be multimodal, the L_2 distance is the Euclidean distance between our prediction and the average of ground-truth annotations. Besides, the minimum distance between our prediction and all ground-truth annotations is also reported. In addition, the average precision (AP) is used to evaluate the performance for is-watching-outside prediction. On this basis, we further report the AP of object detection for the GO-D.

Then, we use the commonly used role *mean average precision* (mAP) to examine the model performance in detecting gaze following and localizing human head simultaneously. Specifically, a HGF detection is considered as true positive if and only if it localizes the human and detects gaze following accurately (*i.e.* the *Interaction-over-Union* (IOU) ratio between the predicted human-head-box and ground-truth is greater than 0.5 while the L_2 distance for GL-D is less than 0.15 and confidence for GO-D is larger than 0.75).

B. Implementation Details

Model structure. We adopt ResNet-50 and ResNet-101 as the CNN backbone of the feature extractor. Both multi-head self-attention and cross-attention has 8 heads. The number of both the human queries and the gaze following queries N_q are set to 20. The number of the human decoder layers L_h and the gaze following decoder layers L_g are both equal to 3.

Model Training. We initialize the network with the parameters of DETR [2]. GTR is trained for 100 epochs using AdamW [28] optimizer with batch size of 16. Specifically, the initial learning rate of the backbone network is set as 10^{-5} while that of the others is set as 10^{-4} , the weight decay is equal to 10^{-4} . Both learning rates are decayed after 80 epochs. For the hyper-parameters of the model, we set $\alpha_{\{h,gl\}}^1$ and $\alpha_{\{h,gl\}}^2$ as 2 and 1 respectively, while revising them for α_{go}^1 and α_{go}^2 . $\beta_{\{hb,gb\}}^1$ and $\beta_{\{hb,gb\}}^2$ are set to 1 and 2.5, respectively. The weights ($\sigma_1 - \sigma_3$) for different cost functions in the loss are set as 2, 1, 1, respectively, while $\eta_1 - \eta_4$ are equal to 2.5, 1, 1, 2. All experiments are conducted on 8 NVIDIA RTX 2080Ti GPUs.

C. Performance Comparison to State-of-the-Art Methods

Gaze location detection. We first verify the effectiveness of our GTR in Table I, which compares several popular GL-D methods on GazeFollowing [31] and VideoAttentionTarget [6] datasets, respectively. As aforementioned, current methods are designed to take human head crops as inputs, we thereby report the results of them on two different setting: “Default” and “Real”. For the former, we directly leverage the manually labeled head crops in dataset annotations. For the latter, we consider the practical scenario to adopt an additional off-the-shelf head detector to individually extract the head crops and feed the predicted results into existing models. In this work, we fine-tune a SSD-based [27] detector using the head annotations in existing dataset, which is followed [6], a competitive GL-D model in existing methods. As the table shown, GTR outperforms current methods on all datasets. Specifically, on GazeFollowing, GTR yields an impressive mAP gain compared to prior methods, ranging from 25% to 35% and leading to a new optimal result (0.604). Moreover, the results of GTR at the “Real” setting even exceed the results of prior methods at the “Default” setting, which are supposed to be their theoretical upper value. Note that our GTR does not require head crops as inputs, but we still report the results of GTR at the “Default” setting by feeding both scene image and head crop into our visual encoder and invalidating the human decoder, which yet leads to an inferior results. Actually, detecting the head crops facilitates the model capability to understanding gaze following, as it allows the model to explicitly attends to head features. Additionally, we find that GTR achieves a more desirable results on VideoAttentionTarget, which can attribute to two major reasons: 1) VideoAttentionTarget is a larger dataset than GazeFollowing, which is preferred by Transformer-based methods. 2) There are more than one human in each image of VideoAttentionTarget while images in GazeFollowing contain only one person. As our model outputs a fixed volume of HGF

instances, fewer human instances in an image potentially refers to a higher fault positive (FP).

Gaze object detection. Table II verifies the effectiveness of GTR for GO-D on GOO [37] dataset. Compared with GaTector [44], GTR achieves a 9.62 AP gain (+19.8%) for GO-D and 0.19 mAP gain (+43.5%) for joint GO-D and human head detection on GOO-Real subset. Moreover, GTR is designed as a single-stage and end-to-end pipeline while prior methods invariably require an additional object detector, which is a fine-tuned YOLO-V4 [1] by following standard protocols. Dispensing with extra detector enforces the model to attends to global contextual semantic, which is further enhanced by attention mechanism in Transformer, promising GTR an excellent performance for GO-D.

D. Importance of Pairwise Detection

In this work, we redefine gaze following detection as a task to jointly detect human head locations and their gaze followings. This subsection aims to validate the importance of such a pairwise detection strategy in terms of model robustness and model efficiency.

Model robustness. An additional human head detector is essential for existing methods since they take both scene image and human head crop as inputs. Nevertheless, in such a cascaded pipeline, the precision of the head detector can easily compromise the performance of the gaze following detection due to potential mis-detection. In practical applications (e.g., video surveillance), image degradations, such as blur, noise, brightness variation, are inevitable. Therefore, we apply several diverse head detectors to analyze model performance in different degradation conditions and report the results in Table III. Here, we adopt VideoAttention [6] equipped with YOLO-V4 as baseline. As the table shown, pairwise detection not only improves the FPS by a large margin (27 vs. 2), but is also more robust with superior performance in different degradation conditions. First, using an extra head detector is a sub-optimal solution since existing models are invariably trained with head crops that are carefully and manually annotated, making they are quite sensitive to the results of the head detector. Secondly, while the influences introduced by image degradation can be partly alleviated by data augmentation in training progress, but it is hard to fine-tune the head detector in real-world applications due to the lack of manually labeled head crops. In comparison, GTR solves gaze following detection in an absolute end-to-end manner, dispensing with the extra head detector, which significantly improves both the results of GL-D (reported *w.r.t* AUC, > 16.9% gain) and GO-D (reported *w.r.t* AP, > 60.6% gain) in all degradation conditions.

Model efficiency. Pairwise detection also introduces high efficiency. Using human head images as input, as existing methods do, limits the ability of detector to predict different people’s gaze followings at the same time. As shown in Fig 3a, as the number of individuals in an identical scene increases, the inference time of existing methods grows extremely. The main reason is that existing methods can predict only one

TABLE I: **Quantitative comparisons on the GazeFollowing and VideoAttentionTarget.** We report the results of different methods *w.r.t* the “Default” and the “Real” two diverse sets, respectively. Specifically, “Default” refers to the utilization of manually annotated head locations from existing datasets, while “real” involves the application of an additional head detector to extract head crops for real world applications.

Method	GazeFollowing [31]							VideoAttentionTarget [6]						
	AUC \uparrow		Average Dist. \downarrow		Min Dist. \downarrow		mAP \uparrow	AUC \uparrow		L2 Dist. \downarrow		AP \uparrow		mAP \uparrow
	Default	Real	Default	Real	Default	Real		Default	Real	Default	Real	Default	Real	
Random	0.504	0.391	0.484	0.533	0.391	0.487	0.104	0.505	0.247	0.458	0.592	0.621	0.349	0.091
Center	0.633	0.446	0.313	0.495	0.230	0.371	0.117	—	—	—	—	—	—	—
Fixed bias	—	—	—	—	—	—	—	0.728	0.522	0.326	0.472	0.624	0.510	0.130
Judd [20]	0.711	—	0.337	—	0.250	—	—	—	—	—	—	—	—	—
GazeFollow [31]	0.878	0.804	0.190	0.233	0.113	0.124	0.457	—	—	—	—	—	—	—
Chong [5]	0.896	0.807	0.187	0.207	0.112	0.120	0.449	0.830	0.791	0.193	0.214	0.705	0.651	0.374
Zhao [49]	—	—	0.147	—	0.082	—	—	—	—	—	—	—	—	—
Lian [25]	0.906	0.881	0.145	0.153	0.081	0.087	0.469	0.837	0.784	0.165	0.172	—	—	0.392
VideoAttention [6]	0.921	0.902	0.137	0.142	0.077	0.082	0.483	0.860	0.812	0.134	0.146	0.853	0.849	0.420
DAM [11]	0.922	—	0.124	—	0.067	—	—	0.905	—	0.108	—	0.896	—	—
GTR (ResNet-50)	0.925	0.928	0.119	0.114	0.063	0.057	0.604	0.927	0.925	0.102	0.093	0.910	0.923	0.584
GTR (ResNet-101)	0.921	0.925	0.121	0.116	0.068	0.064	0.592	0.931	0.936	0.105	0.095	0.914	0.927	0.602

TABLE II: **Quantitative comparisons on the GOO dataset.** We report the results for GL-D on the GOO-Synth subset and the results for GO-D on the GOO-Real subset, which are also based on the aforementioned “Default” and “Real” scenarios.

Method	GOO-Synth							GOO-Real						
	AUC \uparrow		Average Dist. \downarrow		Ang. \downarrow		mAP \uparrow	AP \uparrow		AP $_{50}\uparrow$		AP $_{75}\uparrow$		mAP \uparrow
	Default	Real	Default	Real	Default	Real		Default	Real	Default	Real	Default	Real	
Random	0.497	—	0.454	—	77.0	—	0.076	—	—	—	—	—	—	—
GazeFollow [31]	0.929	0.832	0.162	0.317	33.0	42.6	0.468	35.5	31.6	58.9	54.3	26.7	24.1	0.291
Lian [25]	0.954	0.903	0.107	0.153	19.7	28.1	0.454	35.7	32.1	62.8	58.4	29.4	27.2	0.297
VideoAttention [6]	0.952	0.912	0.075	0.143	15.1	24.5	0.489	36.8	32.4	61.5	56.7	30.8	27.9	0.314
GaTector [44]	0.957	0.918	0.073	0.139	14.9	24.5	0.510	52.25	48.7	91.92	86.4	55.34	52.1	0.437
GTR (ResNet-50)	0.960	0.962	0.071	0.068	14.5	14.2	0.597	58.26	57.12	97.31	96.47	58.42	58.90	0.627
GTR (ResNet-101)	0.954	0.953	0.074	0.070	14.5	14.8	0.588	58.28	58.32	96.93	96.84	59.81	59.79	0.625

human’s gaze target at a time, and the detection process has to be conducted repeatedly when there are more than one human in a same image. On the contrary, our GTR is free with such limitation and its inference time is almost not inflected by the number of humans. In this paper, GTR is designed to detect up to 20 peoples gaze targets at a time. In real world applications, the model can be easily fine-tuned to increase the number of maximum detectable humans by simply changing the value of hyper-parameter N_q .

E. Ablation Study for Model Design

In this subsection, we conduct extensive ablation experiments on VideoAttentionTarget and GOO-Real to validate the effectiveness of our proposed strategies for model design. All experiments are conducted using ResNet-50 as backbone.

Visual encoder. Following DETR [2], our visual encoder is designed as a CNN-based backbone followed by a Transformer encoder, whose impacts are verified in Table IVb. Comparing to feeding original image patches into Transformer, CNN-based feature extractor enables to capture higher-level semantic, leading to a 0.176 (Δ 23.4%) AUC gain for GL-D and a 14.48 (Δ 34.0%) AP gain for GO-D. Moreover, Transformer encoder contributes a 0.243 (Δ 35.5%) AUC improvement and

a 22.90 (Δ 66.9%) AP gain, which are mainly attributed to the self-attention mechanism, thanks to its excellent ability to modeling long range context. We further explore in which cases self-attention especially enables superior performance compared with the current methods. To this end, we split all HGF instances in VideoAttentionTarget test set into bins of size 0.1 on the basis of L_1 distance between the center of human head and her/his gaze location, where the height and width of image have been normalized. We report the results in Fig 3b, where the result of VideoAttention [6] and GaTector [44] are reprinted in “Default” setting, *i.e.*, using the off-the-shelf head crops as inputs. As shown in the Figure, the degraded performance indicates that the gaze following detection tends to be more difficult as the distance grows, and the relative performance gaps between the GTR and the other two detectors correspondingly become more and more evident. Particularly, our GTR shows impressive performance in distant gaze following detection while existing methods are failed. The potential reason for such result is that existing methods deal with limited receptive fields, being weak in extracting long range contextual information and being likely to be dominated by irrelevant information in the distant cases.

Two-branch decoders. We verify the impacts of the two

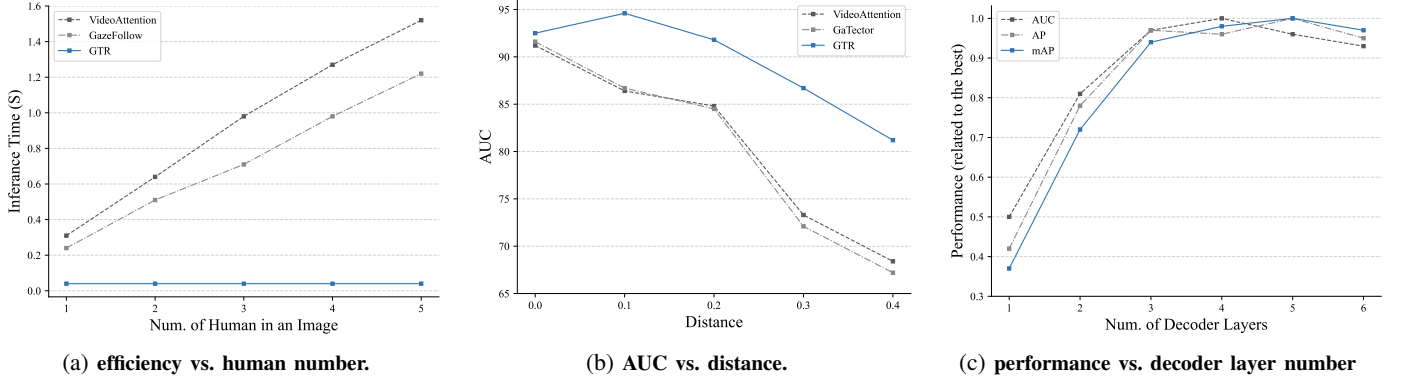


Fig. 3: (a): Inference times of different methods with different numbers of humans in an image. GTR specializes in handling scene image containing multiple humans. (b): AUCs of different methods on different spatial distributions of HGF instances. GTR is more effective at detecting gaze followings that are more distantly distributed. (c): Performance of GTR with different numbers of decoder layers, which shows all metrics’ trends as the number of decoder layers increases, *i.e.*, all metrics are normalized by dividing by their maximum value.

TABLE III: **Performance of using different human head detectors.** We manually degrade the original images in the testing set of VideoAttentionTarget and GOO-Real with several common distortion types. Specifically, “FT” refers to that the training sets of those two dataset are also augmented with these distortion types and the head detectors are further fine-tuned with the head locations in the augmented dataset. “Normal” means that no degeneration image is used.

Method	FT	FPS	Blur			Gaussian Noise			Brightness			Normal		
			AUC	AP	mAP	AUC	AP	mAP	AUC	AP	mAP	AUC	AP	mAP
SSD-based [27]	✗	2	0.729	27.1	0.302	0.706	28.3	0.298	0.738	26.7	0.315	0.789	28.5	0.405
	✓	2	0.774	29.2	0.371	0.767	28.7	0.362	0.784	30.1	0.376	0.812	32.4	0.420
FCHD [43]	✗	3	0.757	27.8	0.336	0.744	29.2	0.328	0.764	27.6	0.341	0.804	30.9	0.409
	✓	3	0.784	30.3	0.385	0.781	31.8	0.325	0.796	30.4	0.392	0.818	33.7	0.424
HeadHunter [36]	✗	1	0.782	29.9	0.341	0.750	30.6	0.332	0.773	29.8	0.352	0.796	32.1	0.412
	✓	1	0.787	31.6	0.389	0.789	33.9	0.384	0.804	33.7	0.410	0.819	35.4	0.424
GTR	✗	27	0.814	53.4	0.442	0.792	54.1	0.438	0.813	54.3	0.451	0.927	57.1	0.584
	✓	27	0.920	55.6	0.567	0.894	53.2	0.513	0.918	55.8	0.496	—	—	—

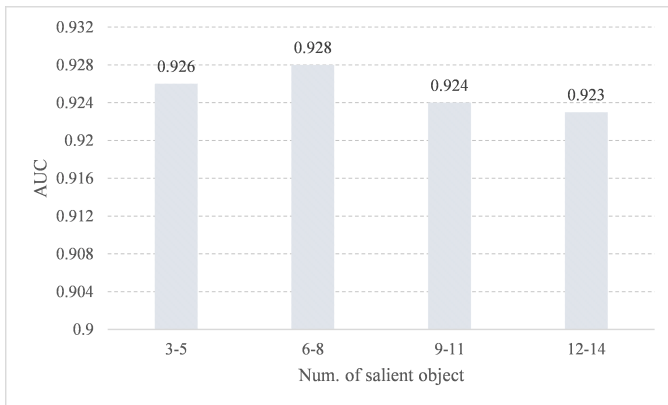


Fig. 4: The impacts of the number of salient objects.

decoders, respectively, *i.e.*, human and gaze following decoder.

1) *Human decoder.* Table IVc verifies the effectiveness of human decoder. Comparing to using a single decoder to predict human heads and understanding their gaze following, additional human decoder introduce a 2.2% AUC gain for GL-D and a 21.1% AP gain for GO-D. Human head detection demands relatively focused receptive field compared to gaze following detection. Therefore, using an additional decoder can effectively reduce the potential semantic ambiguity intro-

duced by the receptive field gaps of these two tasks.

2) *Weight guided embedding.* Jointly Learned with human queries (j -learned in Table IVd) through human decoder, w-GEs are proposed to highlight the potentially salient regions attended by different human queries. As shown in Table IVd, W-GE mechanism brings a 18.5% AUC gain for GL-D and 39.1% AP for GO-D. Interestingly, if we adopt an individual sub-branch to learn w-GE separately (s -learned), the performances of GL-D and GO-D degrade 4.7% and 10.8%, respectively. We conjecture that jointly learning enables an explicit information propagation from human queries to w-GE, thanks to the attention mechanism. We further qualitatively visualize the w-GEs in Fig 5 (the third and the sixth rows), which shows that w-GE roughly highlight the salient regions that potentially be noticed by given human, guiding the subsequent gaze following detection. More examples are illustrated in Fig. 6.

3) *Gaze following decoder.* Our gaze following decoder is designed to iteratively interact with human decoder through a hierarchical architecture. First, if we cut off the connection between human decoder and gaze following decoder (s -dual in Table IVc), the AUC for GL-D degrades 6.9% ($\nabla 0.064$) and the AP for GO-D reduces 14.8% ($\nabla 8.48$). Then, if we adopt an one-shot strategy, *i.e.*, only connecting the last layer of human decoder with the last layer of gaze following decoder, the AUC and AP degrade 3.8% ($\nabla 0.034$) and 13.3% ($\nabla 5.7$),

AUC AP			CNN	T-E	AUC AP		AUC AP		AUC AP			
none	0.782	53.10	✓		0.684	34.22	single	0.907	47.17	none	0.841	39.62
learned	0.925	57.84		✓	0.751	42.64	s-dual	0.863	48.64	s-learned	0.885	52.44
cosine	0.927	57.12	✓	✓	0.927	57.12	j-dual	0.927	57.12	j-learned	0.927	57.12

(a) **Position encoding.** (b) **Visual encoder.** (c) **Decoder structure.** (d) **Weight guided embedding.**

AUC AP			Q_h	w-GE	AUC AP		H	G	Param.	FPS	AUC	AP
last-to-last	0.893	50.42	✓		0.841	39.62	3	3	48.2M	27	0.927	57.12
last-to-all	0.905	53.24		✓	0.863	44.83	3	5	49.6M	24	0.925	58.25
one-to-one	0.927	57.12	✓	✓	0.927	57.12	5	5	56.4M	20	0.911	58.43

(e) **Connection of decoders.** (f) **Gaze following queries.** (g) **Model depths.**

TABLE IV: **GTR ablation experiments** with ResNet-50 on VideoAttentionTarget (AUC for GL-D) and GOO-Real (AP for GO-D). We roundly verify our proposed strategies for model design and compare different possible variants. Default settings are marked in gray.

α_h^1	α_h^2	AP	Recall	α_{gl}^1	α_{gl}^2	AUC	L_2 Dist.	α_{go}^1	α_{go}^2	AP	AP ₅₀
1	1	91.2	73.6	1	1	0.912	0.114	1	1	56.40	96.18
1	2	89.4	70.8	1	2	0.905	0.117	1	2	57.12	96.47
2	1	94.3	73.9	2	1	0.927	0.102	2	1	55.83	96.02

(a) **Human head prediction cost.** (b) **gaze location prediction cost.** (c) **Gaze object prediction cost.**

σ_1	σ_2	σ_3	AUC	AP	mAP	η_1	η_2	η_3	η_4	AUC	AP	mAP
1	1	1	0.922	57.14	0.625	1	1	1	1	0.913	56.41	0.607
2	1	1	0.927	57.12	0.627	2.5	1	1	2	0.927	57.12	0.627
1	2	2	0.914	57.92	0.623	2	2	2	1	0.931	56.42	0.623
						1	1	1	2	0.923	58.04	0.622

(d) **Weights for bipartite matching.** (e) **Weights for objective function.**

TABLE V: **Ablation experiments** for our new loss design, where we aim at verifying the mutual impacts of GL-D and GO-D in our unified framework. Meanwhile, we also explore the effects of regression and classification in different cost functions by changing their weights.

TABLE VI: **GL-D in practical scenario.** “Ang.” refers to the angle between ground-truth gaze direction and the predicted one.

Methods	AUC \uparrow	L_2 Dist. \downarrow	Ang. \downarrow	mAP \uparrow
Gazefollow [31]	0.792	0.213	27.9 $^\circ$	0.407
Lian [25]	0.813	0.167	19.7 $^\circ$	0.441
VideoAttention [6]	0.842	0.145	16.9 $^\circ$	0.476
GaTector [44]	0.837	0.152	17.3 $^\circ$	0.474
GTR	0.938	0.112	11.8$^\circ$	0.562

TABLE VII: **Shared attention detection results on the VideoCoAtt dataset.** The interval detection is evaluated in terms of prediction accuracy while the location task is measured with L_2 distance.

Methods	Accuracy \uparrow	L_2 Dist. \downarrow
Random	50.8	286
Fixed bias	52.4	122
GazeFollow [31]	58.7	102
Gaze+Saliency [29]	59.4	83
Gaze+Saliency+LSTM [16]	66.2	71
Fan [10]	71.4	62
Sumer [35]	78.1	63
VideoAttention [6]	83.3	57
GTR	90.4	41

respectively, as shown in Table IVe. Another intuitive choice is to connect the last layer of human decoder (containing higher-level semantic) with all layers of gaze following decoder,

which yet leads a slight performance degradation ($\nabla 2.4\%$ in AUC and $\nabla 6.8\%$ in AP). We hypothesize that the feature from the last layer of human decoder has a semantic gap between the relative shallow layers in the gaze following decoder. Moreover, as shown in Fig. 4, the human decoder is connected with the gaze-following decoder in a hierarchical and iterative manner, which enables the gaze-following decoder to filter out irrelevant objects gradually. Besides, unlike the human queries are randomly initialized, we explicitly initialize gaze following queries for each layer of gaze following decoder using the human queries and w-GE from the corresponding human decoder layer, whose effects are validated in Table IVf. Intuitively, human queries provide human features while w-GEs introduce the context of potential salient regions, facilitating the learning of cross-attention weights between gaze following queries with global visual features.

3) *Model depth.* Empirically, increasing the depth of decoder, *i.e.*, stacking more layers, is likely to improve performance at the cost of more computational costs. As illustrated by Fig 3c, a 3-layers decoder enables the optimal result for GL-D and that for GO-D is achieved by a 5-layers gaze following decoder. It is because that GL-D is a relative easier task than GO-D. We further try several different combines in depths of two-branch decoders, and find a 3-layer human decoder equipped with a 3-layer gaze following decoder is the optimal solution considering the trade-off in effectiveness and efficiency, as reported in Table IVg.

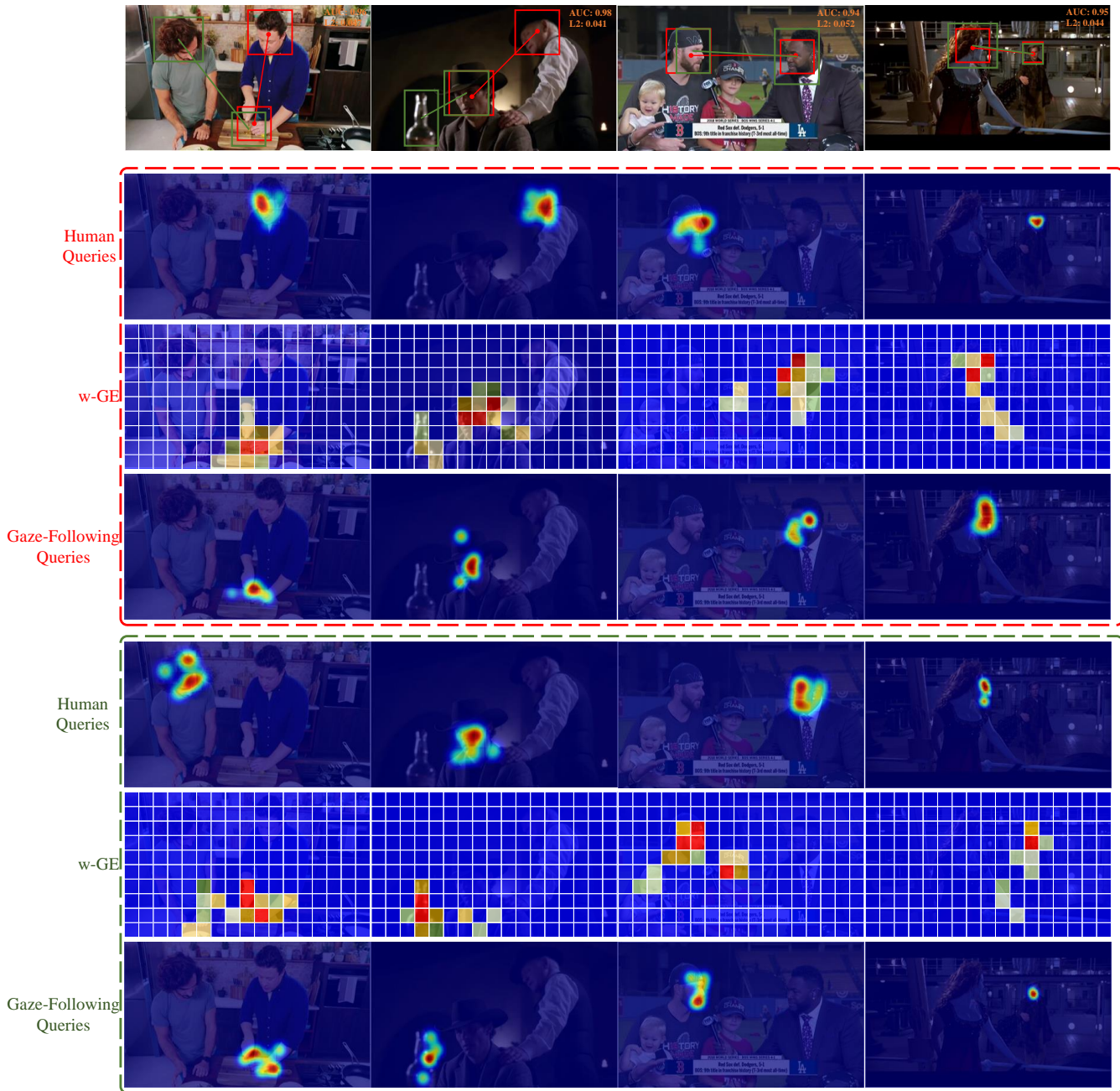


Fig. 5: **Visualization** of human queries (row-II and row-V), w-GE (row-III and row-VI) and gaze following queries (row-IV and row row-VII) in our two-branch decoders. The images are randomly selected from the testing set of VideoAttentionTarget. Attention scores are coded with different colors for different humans. Best viewed in color.

F. Ablation Study for Loss Design

We also conduct extensive ablation experiments to analysis the effectiveness of our proposed new loss function for gaze following detection. We find that for human head detection and GL-D, regression plays a more important role than classification, which are yet reverse for GO-D (Table Va, Vb, Vc). Specially, the “AP” and “Recall” in Table Va are metrics to evaluate the performance of human head detection, where a human head prediction is considered as true positive only if it localizes the human head with an IOU ratio between the predicted head box and the ground-truth one is larger than

0.7. We further compare several different weights for different costs in matching loss and objective loss, the results are reported in Table Vd and Table Ve, respectively. Actually, for close to the last decade, gaze following detection has always been dominated by distance-based loss, such as L_1 and L_2 loss. We hope our new loss can provide some desirable points for gaze following community.

G. Generalization Performance

Practical application. To evaluate the GTR’s generalization performance in practical scenarios, we randomly select 15,000



Fig. 6: **Visualization** of detection results of GTR. The images are selected from GazeFollowing (in green rectangle), VideoAttentionTarget (in brown rectangle), GOO-Synth (in blue rectangle) and GOO-Real (in red rectangle).

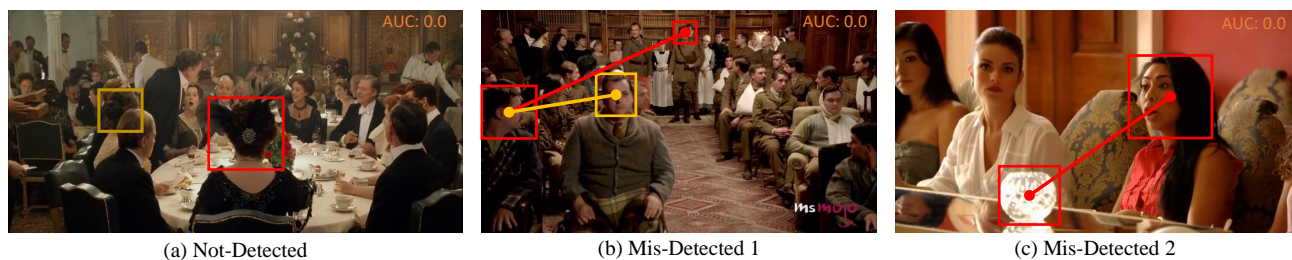


Fig. 7: **Failed cases**. In (a), GTR fails to detect the human head due to the lack of discriminative facial features (the red one) and occlusion (the yellow one). In (b), the gaze location are mis-predicted (the red one is the ground-truth) due to the salient object in the foreground (the yellow one). In (c), the salient object misguides the prediction for the human is looking outside of the image. The images are randomly selected from the testing set of VideoAttentionTarget and GazeFollowing.

image from DL Gaze dataset [25], which records the daily activities of 16 volunteers in 4 diverse scenes and the ground-truth annotations are labeled by the observers in the videos. We compare the performance of different models by training them just with the VideoAttentionTarget dataset and then applying

them for DL Gaze without fine-tuning. As the quantitative results reported in Table VI, our GTR outperforms all state-of-the-art methods by a significant margin, demonstrating its impressive performance in practical applications.

Shared attention detection. With the ability to detect gaze

locations of different people simultaneously, GTR are natively able to understanding shared attention in social scenes. We report the results in terms of accuracy for interval detection of shared attention and L_2 distance for location prediction on the VideoCoAtt [10] by following [6]. VideoCoAtt contains 113,810 tset frames that are annotated with the target location when it is simultaneously attended by two or more people. As can be seen from Table VII, GTR shows a excellent potntial value of recognizing higher-lever social gaze.

V. DISCUSSION

Transformer demonstrates impressive capability in gaze following detection. We conjecture the reasons are twofold: 1) Long range context modeling is essential in gaze following detection. Compared to CNN with limited receptive field, the global attention mechanism ensures Transformer to capture holistic scene feature, providing crucial cues to reason possible gaze location. 2) Interactions between holistic scene contexts and head pose features are important. We reframe gaze following detection task as detecting human head locations and their gaze followings simultaneously, which implicitly enforces the model to learn the interactions between these two different features. Besides, we design the decoder of our GTR as two parallel branches, one of which aims for head detection and another one is responsible for gaze following detection. Meanwhile, these two branch is connected in a hierarchical and iterative manner, which explicitly enables a strong interaction between holistic scene contexts and head features. Besides the model design, it is our belief that defining gaze following detection task as simultaneously detecting human head locations and their gaze following is more reasonable, since manually labeled head locations are unavailable in practical scenarios. Moreover, it allows us to detect multiple humans' gaze followings at once, saving computational complexity and being more efficient.

However, GTR sometimes may be failed, and we exemplify some representative failed cases in Fig. 5. In some scenarios, such as the human head is partly occluded or he/she turns his/her back to the camera, the GTR may fails to localize the human head due to the missing of discriminative facial features. Actually, occlusion has always plagued detection system and many excellent methods [21, 51] have been proposed to solve it, among which data augmentation may be one of effective solutions for the GTR. In terms of gaze following detection, GTR sometimes may be deluded by the foreground objects since they are likely to be more salient. In this case, using additional cues, *e.g.*, depths [11], can be a great choice to guide the GTR.

VI. CONCLUSION

In this paper, we present a new Transformer-based method for the task of gaze following detection, named as GTR. GTR models global contextual information, being designed to localize all humans' head crops as well as to detect their gaze following simultaneously. GTR unites gaze location detection and gaze object detection in a unified framework, which is also the first single-stage pipeline where the model can be trained in

a fully end-to-end manner. Extensive experiments validate its impressive performance in both effectiveness and efficiency. Besides, GTR shows desirable potential for understanding gaze behavior in naturalistic human interactions. We hope our method will be useful for human activity understanding research.

REFERENCES

- [1] Alexey Bochkovskiy, Chien-Yao Wang, and Hong-Yuan Mark Liao. Yolov4: Optimal speed and accuracy of object detection. *arXiv preprint arXiv:2004.10934*, 2020.
- [2] Nicolas Carion, Francisco Massa, Gabriel Synnaeve, Nicolas Usunier, Alexander Kirillov, and Sergey Zagoruyko. End-to-end object detection with transformers. In *ECCV*, 2020.
- [3] Hanqing Chen, Yunhe Wang, Tianyu Guo, Chang Xu, Yiping Deng, Zhenhua Liu, Siwei Ma, Chunjing Xu, Chao Xu, and Wen Gao. Pre-trained image processing transformer. In *CVPR*, 2021.
- [4] Wenhe Chen, Hui Xu, Chao Zhu, Xiaoli Liu, Yinghua Lu, Caixia Zheng, and Jun Kong. Gaze estimation via the joint modeling of multiple cues. *IEEE TCSVT*, 2021.
- [5] Eunji Chong, Nataniel Ruiz, Yongxin Wang, Yun Zhang, Agata Rozga, and James M Rehg. Connecting gaze, scene, and attention: Generalized attention estimation via joint modeling of gaze and scene saliency. In *ECCV*, 2018.
- [6] Eunji Chong, Yongxin Wang, Nataniel Ruiz, and James M Rehg. Detecting attended visual targets in video. In *CVPR*, 2020.
- [7] Victor Delvigne, Hazem Wannous, Thierry Dutoit, Laurence Ris, and Jean-Philippe Vandeborre. Phydac: Physiological dataset assessing attention. *IEEE TCSVT*, 2021.
- [8] Alexey Dosovitskiy, Lucas Beyer, Alexander Kolesnikov, Dirk Weissenborn, Xiaohua Zhai, Thomas Unterthiner, Mostafa Dehghani, Matthias Minderer, Georg Heigold, Sylvain Gelly, et al. An image is worth 16x16 words: Transformers for image recognition at scale. In *ICLR*, 2021.
- [9] Huiyu Duan, Wei Shen, Xiongkuo Min, Danyang Tu, Jing Li, and Guangtao Zhai. Saliency in augmented reality. In *ACM MM*, 2022.
- [10] Lifeng Fan, Yixin Chen, Ping Wei, Wenguan Wang, and Song-Chun Zhu. Inferring shared attention in social scene videos. In *CVPR*, 2018.
- [11] Yi Fang, Jiapeng Tang, Wang Shen, Wei Shen, Xiao Gu, Li Song, and Guangtao Zhai. Dual attention guided gaze target detection in the wild. In *CVPR*, 2021.
- [12] Yanliang Ge, Qiao Zhang, Tian-Zhu Xiang, Cong Zhang, and Hongbo Bi. Tcnet: Co-salient object detection via parallel interaction of transformers and cnns. *IEEE TCSVT*, 2022.
- [13] Jian Guan, Liming Yin, Jianguo Sun, Shuhan Qi, Xuan Wang, and Qing Liao. Enhanced gaze following via object detection and human pose estimation. In *ICMM*, 2020.
- [14] Kaiming He, Xiangyu Zhang, Shaoqing Ren, and Jian Sun. Deep residual learning for image recognition. In *CVPR*, 2016.
- [15] Kaiming He, Xiangyu Zhang, Shaoqing Ren, and Jian Sun. Deep residual learning for image recognition. In *CVPR*, 2016.
- [16] Sepp Hochreiter and Jürgen Schmidhuber. Long short-term memory. *Neural computation*, 1997.
- [17] Kenneth Holmqvist, Marcus Nyström, Richard Andersson, Richard Dewhurst, Halszka Jarodzka, and Joost Van de Weijer. *Eye tracking: A comprehensive guide to methods and measures*. 2011.
- [18] Xiaodi Hou and Liqing Zhang. Saliency detection: A spectral residual approach. In *CVPR*, 2007.
- [19] Zhengxi Hu, Kunxu Zhao, Bohan Zhou, Hang Guo, Shichao Wu, Yuxue Yang, and Jingtai Liu. Gaze target estimation inspired by interactive attention. *IEEE TCSVT*, 2022.
- [20] Tilke Judd, Krista Ehinger, Frédo Durand, and Antonio Torralba. Learning to predict where humans look. In *ICCV*, 2009.
- [21] Jung Uk Kim, Jungsu Kwon, Hak Gu Kim, and Yong Man Ro. Bbc net: Bounding-box critic network for occlusion-robust object detection. *IEEE TCSVT*, 2019.

- [22] Kyle Krafka, Aditya Khosla, Petr Kellnhofer, Harini Kannan, Suchendra Bhandarkar, Wojciech Matusik, and Antonio Torralba. Eye tracking for everyone. In *CVPR*, 2016.
- [23] Harold W Kuhn. The hungarian method for the assignment problem. *Naval Research Logistics Quarterly*, 1955.
- [24] George Leifman, Dmitry Rudoy, Tristan Swedish, Eduardo Bayro-Corrochano, and Ramesh Raskar. Learning gaze transitions from depth to improve video saliency estimation. In *CVPR*, 2017.
- [25] Dongze Lian, Zehao Yu, and Shenghua Gao. Believe it or not, we know what you are looking at! In *ACCV*, 2018.
- [26] Tsung-Yi Lin, Michael Maire, Serge Belongie, James Hays, Pietro Perona, Deva Ramanan, Piotr Dollár, and C Lawrence Zitnick. Microsoft coco: Common objects in context. In *ECCV*, 2014.
- [27] Wei Liu, Dragomir Anguelov, Dumitru Erhan, Christian Szegedy, Scott Reed, Cheng-Yang Fu, and Alexander C Berg. Ssd: Single shot multibox detector. In *ECCV*, 2016.
- [28] Ilya Loshchilov and Frank Hutter. Decoupled weight decay regularization. In *ICLR*, 2017.
- [29] Junting Pan, Elisa Sayrol, Xavier Giro-i Nieto, Kevin McGuinness, and Noel E O'Connor. Shallow and deep convolutional networks for saliency prediction. In *CVPR*, 2016.
- [30] Manoranjan Paul and Md Musfequs Salehin. Spatial and motion saliency prediction method using eye tracker data for video summarization. *IEEE TCSVT*, 2018.
- [31] Adria Recasens, Aditya Khosla, Carl Vondrick, and Antonio Torralba. Where are they looking? In *NIPS*, 2015.
- [32] Hamid Rezaatofighi, Nathan Tsoi, JunYoung Gwak, Amir Sadeghian, Ian Reid, and Silvio Savarese. Generalized intersection over union: A metric and a loss for bounding box regression. In *CVPR*, 2019.
- [33] Nataliya Shapovalova, Michalis Raptis, Leonid Sigal, and Greg Mori. Action is in the eye of the beholder: Eye-gaze driven model for spatio-temporal action localization. *NIPS*, 2013.
- [34] Robin Strudel, Ricardo Garcia, Ivan Laptev, and Cordelia Schmid. Segmenter: Transformer for semantic segmentation. *arXiv preprint arXiv:2105.05633*, 2021.
- [35] Omer Sumer, Peter Gerjets, Ulrich Trautwein, and Enkelejda Kasneci. Attention flow: End-to-end joint attention estimation. In *CVPR*, 2020.
- [36] Ramana Sundararaman, Cedric De Almeida Braga, Eric Marchand, and Julien Pettre. Tracking pedestrian heads in dense crowd. In *CVPR*, 2021.
- [37] Henri Tomas, Marcus Reyes, Raimarc Dionido, Mark Ty, Jonric Mirando, Joel Casimiro, Rowel Atienza, and Richard Guinto. Goo: A dataset for gaze object prediction in retail environments. In *CVPRW*, 2021.
- [38] Danyang Tu, Xiongkuo Min, Huiyu Duan, Guodong Guo, Guangtao Zhai, and Wei Shen. End-to-end human-gaze-target detection with transformers. In *CVPR*, 2022.
- [39] Danyang Tu, Xiongkuo Min, Huiyu Duan, Guodong Guo, Guangtao Zhai, and Wei Shen. Iwin: Human-object interaction detection via transformer with irregular windows. In *ECCV*, 2022.
- [40] Danyang Tu, Wei Sun, Guangtao Zhai, and Wei Shen. Agglomerative transformer for human-object interaction detection. *arXiv preprint arXiv:2308.08370*, 2023.
- [41] Danyang Tu, Wei Sun, Guangtao Zhai, Wei Shen, et al. Video-based human-object interaction detection from tubelet tokens. In *NIPS*, 2022.
- [42] Ashish Vaswani, Noam Shazeer, Niki Parmar, Jakob Uszkoreit, Llion Jones, Aidan N Gomez, Łukasz Kaiser, and Illia Polosukhin. Attention is all you need. In *NIPS*, 2017.
- [43] Aditya Vora and Vinay Chilaka. Fchd: Fast and accurate head detection in crowded scenes. *arXiv preprint arXiv:1809.08766*, 2018.
- [44] Binglu Wang, Tao Hu, Baoshan Li, Xiaojuan Chen, and Zhijie Zhang. Gatecor: A unified framework for gaze object prediction. In *CVPR*, 2022.
- [45] Bingjie Xu, Junnan Li, Yongkang Wong, Qi Zhao, and Mohan S Kankanhalli. Interact as you intend: Intention-driven human-object interaction detection. *IEEE TMM*, 2019.
- [46] Qiong Yan, Li Xu, Jianping Shi, and Jiaya Jia. Hierarchical saliency detection. In *CVPR*, 2013.
- [47] Ruohan Zhang, Akanksha Saran, Bo Liu, Yifeng Zhu, Sihang Guo, Scott Niekum, Dana Ballard, and Mary Hayhoe. Human gaze assisted artificial intelligence: A review. In *IJCAI*, 2020.
- [48] Xucong Zhang, Yusuke Sugano, Mario Fritz, and Andreas Bulling. Appearance-based gaze estimation in the wild. In *CVPR*, 2015.
- [49] Hao Zhao, Ming Lu, Anbang Yao, Yurong Chen, and Li Zhang. Learning to draw sight lines. *IJCV*, 2019.
- [50] Sixiao Zheng, Jiachen Lu, Hengshuang Zhao, Xiatian Zhu, Zekun Luo, Yabiao Wang, Yanwei Fu, Jianfeng Feng, Tao Xiang, Philip HS Torr, et al. Rethinking semantic segmentation from a sequence-to-sequence perspective with transformers. In *CVPR*, 2021.
- [51] Chunluan Zhou and Junsong Yuan. Occlusion pattern discovery for object detection and occlusion reasoning. *IEEE TCSVT*, 2019.
- [52] Wangjiang Zhu and Haoping Deng. Monocular free-head 3d gaze tracking with deep learning and geometry constraints. In *CVPR*, 2017.
- [53] Xizhou Zhu, Weijie Su, Lewei Lu, Bin Li, Xiaogang Wang, and Jifeng Dai. Deformable detr: Deformable transformers for end-to-end object detection. In *ICLR*, 2020.
- [54] Zhiwei Zhu and Qiang Ji. Eye gaze tracking under natural head movements. In *CVPR*, 2005.